

A Three Dimensional Alfvénic Pulse in a Transversely Inhomogeneous Medium

D. Tsiklauri and V.M. Nakariakov

Physics Department, University of Warwick, Coventry, CV4 7AL, U.K.

Received 2001 / Accepted 2001

Abstract. Interaction of incompressible and compressible MHD fluctuations on a one-dimensional plasma inhomogeneity, transverse to the magnetic field, is considered in the three-dimensional regime. An initially incompressible (Alfvénic) MHD fluctuation generates, by linear coupling, compressible (magnetoacoustic) fluctuations. In the initial stage of the interaction, the efficiency of the coupling is enhanced by phase mixing of the incompressible mode. In the developed stage of phase mixing, the interaction saturates and both incompressible and compressible fluctuations approach a quasi-stationary state. The saturation levels of density fluctuations and incompressible fluctuations tend to become equal as the linear coupling strength increases.

Key words. Magnetohydrodynamics(MHD)– waves – Sun: activity – Sun: Solar wind

1. Introduction

Problems of heating of the open corona of the Sun and acceleration of the solar wind are closely related with the interaction of linearly incompressible Alfvén waves with compressible magnetoacoustic waves. Investigation of coupling mechanisms between the modes is of prime importance because, on one hand, the Alfvén waves are usual candidates of energy transport from the lower layers of the solar atmosphere to the corona, and, on the other, compressible perturbations are subject to much more efficient dissipation than the incompressible Alfvén waves (see, e.g., Narain & Ulmschneider (1996)). Also, the compressive waves, as opposed to the Alfvén waves, can transport energy across the magnetic field, due to the fact that their propagation in space is not constrained by the field lines.

The original idea of the phase mixing of *incompressible* Alfvén waves (Hayvaerts & Priest (1983)) was based on the following argument: when plasma has a density gradient perpendicular to the magnetic field, local Alfvén speed is a function of the transverse coordinate. Thus, when an Alfvén wave propagates along the field its perturbations on the adjacent field lines become out of phase. This stretching of Alfvén wave front creates progressively smaller spatial scales across the field. In turn, because the dissipation is proportional to the wave number squared, phase mixing leads to enhanced dissipation of the Alfvén wave directly. However, in addition,

as demonstrated by Malara, Petkaki & Veltri (1996), Nakariakov et al. (1997), Nakariakov et al. (1998), Botha et al. (2000), Tsiklauri, Arber & Nakariakov (2001), Tsiklauri, Nakariakov & Arber (2002), phase mixing of linearly polarized, plane Alfvén waves in the *compressible* plasma, in the *nonlinear* regime leads to the generation of fast magnetoacoustic waves. However, it was established, in 2.5D geometry, for the harmonic Alfvén wave Botha et al. (2000), and for a wide spectrum Alfvén pulse by Tsiklauri, Arber & Nakariakov (2001) that compressive perturbations, which are initially absent from the system, do not grow to a substantial fraction of the initial Alfvén wave due the destructive wave interference effect.

Since observations established the existence of *large amplitude* Alfvén waves in the solar wind, we further extended our previous work Tsiklauri, Arber & Nakariakov (2001) for the strongly non-linear amplitudes Tsiklauri, Nakariakov & Arber (2002). We simulated numerically, in 2.5D geometry, the interaction of a *strongly non-linear*, linearly polarized, plane Alfvénic pulse with a one-dimensional, perpendicular to the magnetic field, plasma density inhomogeneity. Among other facts we established then that the maximum generated amplitude of transverse compressive wave, up to about 40 % of the initial Alfvén wave amplitude, is reached for about $\beta = 0.5$.

There is yet another possibility to generate fast (and slow) magnetoacoustic waves, which becomes possible even in the linear regime – that is a linear coupling of an oblique Alfvén wave to fast and slow magnetoacoustic

waves. This becomes possible in the presence of non-zero gradients in the wave field in the third direction, perpendicular to both the magnetic field and the gradient of the Alfvén speed. *The efficiency of coupling is proportional to a product of the characteristic scales of the waves in two perpendicular directions. As the gradient of the transverse to the magnetic field inhomogeneity is increased by the phase mixing, the efficiency of the linear coupling between the Alfvén and compressive modes should also be increased accordingly. One of the aims of this work is to investigate, in 3D geometry, whether the linear coupling efficiency is affected by the destructive wave interference effect as it has been established in the 2.5D weakly non-linear case Tsiklauri, Arber & Nakariakov (2001).*

In this work we consider fully three dimensional geometry and study the linear coupling of phase mixed Alfvén waves to the longitudinal and transverse compressive waves. Similar coupling mechanism was studied by De Groof & Goossens (2000) in the context of resonant absorption of MHD waves in coronal loops as a heating mechanism. However, our treatment is more general as we perform a direct numerical 3D simulation without resorting to Fourier transform in time and y direction. Besides, they used a harmonic form of the initial perturbation as opposed to our spatially localized, Gaussian, one. Recently, Hood, Brooks & Wright (2002) showed that the wide spectrum regime of phase mixing can be quite different from the harmonic one, as in fact, phase mixing of localized Alfvén pulses results in a slower, algebraic, damping as opposed to the standard exponential damping of harmonic Alfvén waves, which suggest that localized Alfvénic perturbations will transport energy higher into the corona than harmonic ones. Such Alfvénic perturbations could be generated e.g. by some transient events such as solar flares, coronal mass ejections, etc. While most of the phase-mixing studies concentrated on harmonic Alfvén perturbations (e.g. Hayvaerts & Priest (1983), Hood, Ireland & Priest (1997), Hood et al. (1997), Nakariakov et al. (1998), Ruderman, Nakariakov & Roberts (1998), DeMoortel et al. (1999), DeMoortel, Hood & Arber (2000), Grappin, Léorat & Buttighoffer (2000), Botha et al. (2000)) only few considered spatially localized ones (Nakariakov et al. (1997), Tsiklauri, Arber & Nakariakov (2001), Tsiklauri, Nakariakov & Arber (2002), Hood, Brooks & Wright (2002)).

An additional motivation to this study is connected with the growing interest to the problem of interaction of MHD waves with 2D and 3D plasma structures and irregularities, as the coronal and wind plasmas are observed to be structured in all three dimensions. 2D and 3D structuring can dramatically affect properties of MHD waves. In particular, as it was shown in the incompressible regime by Similon & Sudan (1989) and confirmed in numerical experiments performed by Petkaki, Malara & Veltri (1998) and Malara, Petkaki & Veltri (2000), the structuring dramatically increases the efficiency of wave dissipation.

However, in those studies, the effects of MHD wave coupling were not taken into account, as only the incompressible regime has been considered. From this point of view, our investigation of the interaction of a 3D Alfvénic pulse with a 1D plasma inhomogeneity in the compressible regime provides the necessary building element of the general theory of MHD wave interaction with plasma inhomogeneities.

We show that when initial Alfvénic perturbation interacts with plasma inhomogeneity, it generates fast and slow magnetosonic waves (through linear coupling). The Alfvénic pulse, initially incompressible, evolves to an MHD pulse which contains both the compressible and incompressible components. In spite of the continuous action of phase mixing, the MHD pulse reaches a new quasi-steady saturated state. We found that the saturation level depends on the plasma- β parameter, and the saturation levels of density fluctuations and incompressible fluctuations tend to become equal as the linear coupling strength increases.

The paper is organized as follows: in section 2 we formulate our model. In section 3 we present the results of numerical simulation, while we close in section 4 with the discussion of main results.

2. The model

In our model we use equations ideal MHD

$$\rho \frac{\partial \mathbf{V}}{\partial t} + \rho(\mathbf{V} \cdot \nabla) \mathbf{V} = -\nabla p - \frac{1}{4\pi} \mathbf{B} \times \text{curl} \mathbf{B}, \quad (1)$$

$$\frac{\partial \mathbf{B}}{\partial t} = \text{curl}(\mathbf{V} \times \mathbf{B}), \quad (2)$$

$$\frac{\partial p}{\partial t} + \mathbf{V} \cdot \nabla p + \gamma p \nabla \cdot \mathbf{V} = 0, \quad (3)$$

where \mathbf{B} is the magnetic field, \mathbf{V} is plasma velocity, ρ is plasma mass density, and p is plasma thermal pressure. In what follows we use 5/3 for the value of γ .

We solve equations (1)-(3) in Cartesian coordinates (x, y, z) . Note that as we solve a fully 3D problem we retain variation in the y -direction, i.e. $(\partial/\partial y \neq 0)$. The equilibrium state is taken to be an inhomogeneous plasma of density $\rho_0(x)$ and a uniform magnetic field B_0 in the z -direction. We consider a plasma configuration similar to the one investigated in Malara, Petkaki & Veltri (1996), Nakariakov et al. (1997), Nakariakov et al. (1998), Botha et al. (2000), Tsiklauri, Arber & Nakariakov (2001), i.e. the plasma has a one-dimensional inhomogeneity in the equilibrium density $\rho_0(x)$ and temperature $T_0(x)$. The unperturbed thermal pressure, p_0 , is taken to be constant everywhere.

Next, we do usual linearization of the Eqs. (1)-(3) and write them in component form as following

$$\rho_0(x) \frac{\partial V_x}{\partial t} + \frac{\partial p}{\partial x} - \frac{B_0}{4\pi} \left(\frac{\partial B_x}{\partial z} - \frac{\partial B_z}{\partial x} \right) = 0, \quad (4)$$

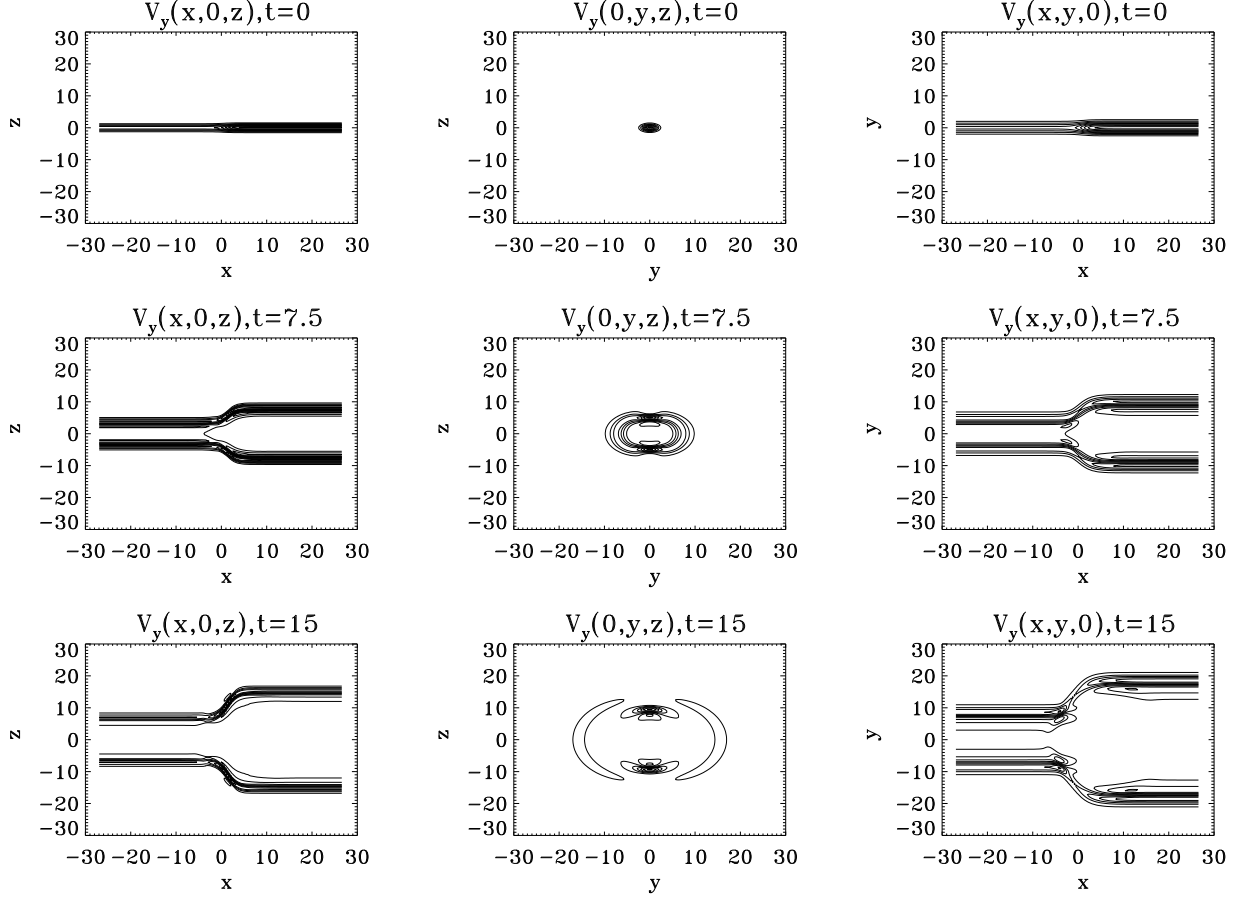


Fig. 1. Contour plots of V_y through three cross-sections at three time snapshots. Here, $\beta = 0.5$, $k_y = 0.6$, $k_z = 1.0$.

$$\rho_0(x) \frac{\partial V_y}{\partial t} + \frac{\partial p}{\partial y} - \frac{B_0}{4\pi} \left(\frac{\partial B_z}{\partial y} - \frac{\partial B_y}{\partial z} \right) = 0, \quad (5)$$

$$\rho_0(x) \frac{\partial V_z}{\partial t} + \frac{\partial p}{\partial z} = 0, \quad (6)$$

$$\frac{\partial B_x}{\partial t} - B_0 \frac{\partial V_x}{\partial z} = 0, \quad (7)$$

$$\frac{\partial B_y}{\partial t} - B_0 \frac{\partial V_y}{\partial z} = 0, \quad (8)$$

$$\frac{\partial B_z}{\partial t} + B_0 \left(\frac{\partial V_x}{\partial x} + \frac{\partial V_y}{\partial y} \right) = 0, \quad (9)$$

$$\frac{\partial p}{\partial t} + \gamma p_0 \left(\frac{\partial V_x}{\partial x} + \frac{\partial V_y}{\partial y} + \frac{\partial V_z}{\partial z} \right) = 0. \quad (10)$$

It is useful to re-write Eqs. (4)-(10) in a form of three coupled wave equations as following

$$\begin{aligned} & [\partial_{tt}^2 - (c_s^2(x) + c_A^2(x)) \partial_{xx}^2 - c_A^2(x) \partial_{zz}^2] V_x \\ & - [(c_s^2(x) + c_A^2(x)) \partial_{xy}^2] V_y - [c_s^2(x) \partial_{xz}^2] V_z = 0, \end{aligned} \quad (11)$$

$$\begin{aligned} & [\partial_{tt}^2 - (c_s^2(x) + c_A^2(x)) \partial_{yy}^2 - c_A^2(x) \partial_{zz}^2] V_y \\ & - [(c_s^2(x) + c_A^2(x)) \partial_{xy}^2] V_x - [c_s^2(x) \partial_{yz}^2] V_z = 0, \end{aligned} \quad (12)$$

$$\begin{aligned} & [\partial_{tt}^2 - c_s^2(x) \partial_{zz}^2] V_z - [c_s^2(x) \partial_{xz}^2] V_x \\ & - [c_s^2(x) \partial_{yz}^2] V_y = 0, \end{aligned} \quad (13)$$

where $c_A(x) = B_0 / \sqrt{4\pi\rho_0(x)}$ and $c_s(x) = \sqrt{\gamma p_0 / \rho_0(x)}$ denote local Alfvén and sound speeds respectively.

We solve Eqs.(4)-(10) numerically after re-writing them in a dimensionless form using following normalization: $B_{x,y,z} = B_0 \bar{B}_{x,y,z}$, $(x, y, z) = a_0(\bar{x}, \bar{y}, \bar{z})$, $c_A(x) = B_0 / \sqrt{4\pi\rho_0(x)} = c_A^0 / \sqrt{3 - 2 \tanh(\lambda x)}$, $t = (a_0 / c_A^0) \bar{t}$, $V_{x,y,z} = c_A^0 \bar{V}_{x,y,z}$. Note, that $c_s(x) = \sqrt{\gamma\beta/2} c_A(x) \equiv \sqrt{\chi} c_A(x)$, where β stands for the ratio of thermal and magnetic pressures $\beta = p_0 / (B_0^2 / 8\pi)$. Here, λ is a free parameter which controls the steepness of the density profile gradient. In our simulations we use $\lambda = 0.5$. In what follows we omit bars on top of the physical quantities.

3. Numerical Results

In order to solve Eqs.(4)-(10) numerically we have written a new numerical code *dt4dx10*, which uses a high order finite difference scheme. Namely, it evaluates 10-th order centered spatial derivatives, and advances solution in time using 4-th order Runge-Kutta algorithm. Therefore, *dt4dx10* is $O[(\Delta t/T)^4]$ accurate in time and $O[(\max(\Delta x, \Delta y, \Delta z)/L)^{10}]$ accurate in space, with T and

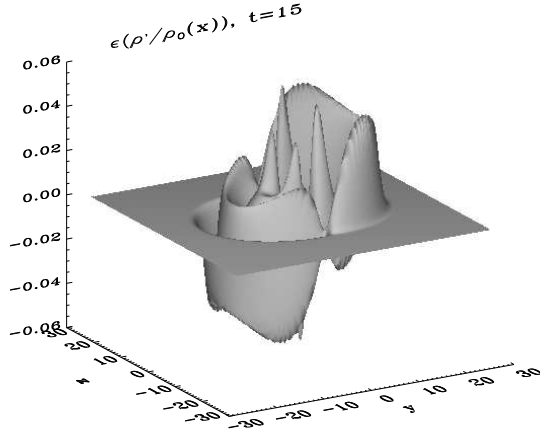


Fig. 2. Snapshots of $\epsilon(\rho'/\rho_0(x))$ at $t = 15$ through $x = 0$ cross-section. Here, $\beta = 0.5$, $k_y = 0.6$, $k_z = 1.0$.

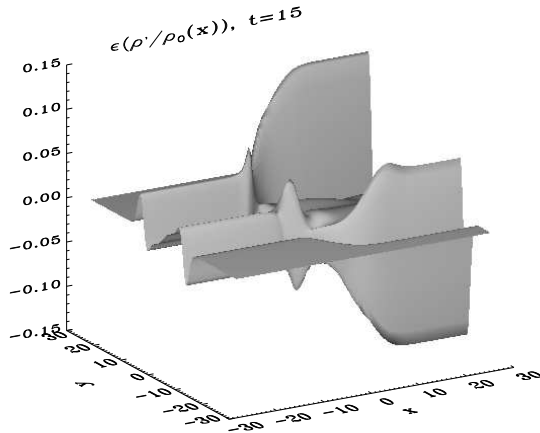


Fig. 3. Snapshots of $\epsilon(\rho'/\rho_0(x))$ at $t = 15$ through $z = 0$ cross-section. Here, $\beta = 0.5$, $k_y = 0.6$, $k_z = 1.0$.

L denoting run time and linear size of the simulation domain. The use of such a high-order numerical approach was motivated by the very nature of the problem considered, as development of phase mixing leads to the generation of very steep profiles in the wave front.

The simulation cube size is set by the limits $-25.0 \leq x \leq 25.0$, $-25.0 \leq y \leq 25.0$ and $-25.0 \leq z \leq 25.0$. Only when k_y -parameter was fixed at 0.1 (see below) we had to double our simulation cube size and double the run-time in order to reach the saturation in the generated density perturbation amplitude. In this case we doubled the number of grid points each direction in order to preserve the same simulation resolution. Boundary conditions used in all our simulations are zero-gradient in all three spatial dimensions.

We have performed calculation on various resolutions in attempt to achieve convergence of the results. The graphical results presented here are for the spatial resolution 128^3 , which refers to number of grid points in x , y and z directions respectively. We have also performed cal-

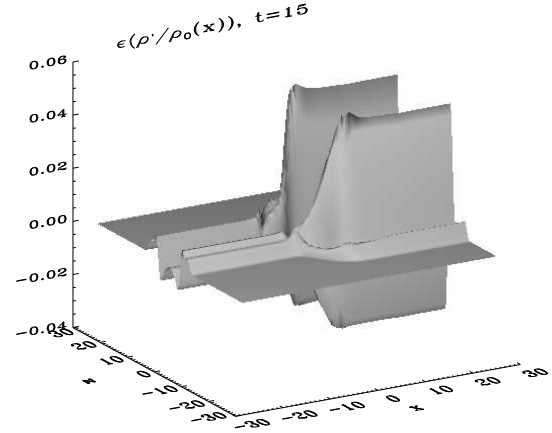


Fig. 4. Snapshots of $\epsilon(\rho'/\rho_0(x))$ at $t = 15$ through $y = 0$ cross-section. Here, $\beta = 0.5$, $k_y = 0.6$, $k_z = 1.0$.

ulation on the spatial resolution 256^3 and we found that the results converge perfectly. This is understandable due to the high order of the scheme even for the 128^3 resolution time-error, $O[(\Delta t/T)^4] \approx 7 \times 10^{-8}$, and spatial-error, $O[(\max(\Delta x, \Delta y, \Delta z)/L)^{10}] \approx 8 \times 10^{-22}$. Since a 256^3 resolution run takes about 8 hours on Compaq ES40 with eight EV6 500-MHz processors, while a 128^3 resolution takes only 1 h on Compaq ES40 with four EV6 500-MHz processors producing the same results, we opted for the latter, less CPU-consuming, alternative.

We set up the code in such a way that initially longitudinal and transverse compressive perturbations as well as density perturbation are absent. In the numerical simulations the Alfvén perturbation is initially a plane (with respect to x -coordinate) pulse, which has a Gaussian structure in y and z -coordinates

$$V_y(x, y, z, t = 0) = c_A(x) \exp(-(k_y y)^2 - (k_z z)^2). \quad (14)$$

Here, k_y and k_z are free parameters which control the strength of gradients in y and z direction of the initial Alfvénic perturbation. As the problem considered is linear, the wave amplitude can be taken to be normalized to unity.

In Fig. 1 we present time evolution of the initial Alfvénic pulse (V_y) through three cross-sections. Namely, left column shows three snapshots of V_y through $y = 0$ cross-section, middle column shows three snapshots of V_y through $x = 0$ cross-section, while right column shows three snapshots of V_y through $z = 0$ cross-section. What we gather from this graph is as following:

- $y = 0$ cross-section: the initial Alfvénic pulse, which is plain with respect to x -coordinate, is split in two D’Alembert’s solutions, with half of the amplitudes, traveling in two opposite directions along the magnetic field. Because the unperturbed density is inhomogeneous across the magnetic field (in x -direction) the local Alfvén speed depends upon x . Thus, the Alfvénic pulse is phase-mixed and its initially plain front is

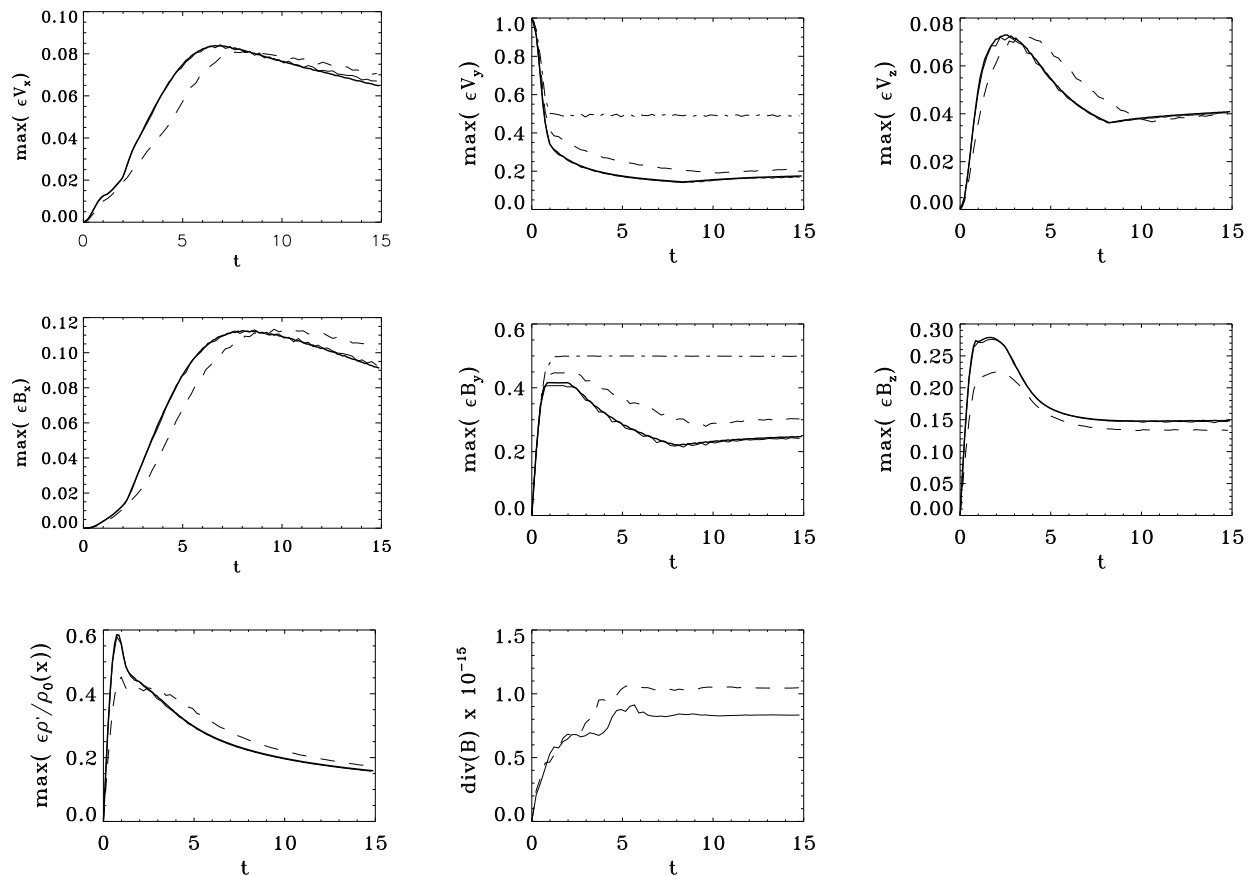


Fig. 5. Maximum of the absolute values over the whole 3D simulation box of all physical quantities as a function of time. Here, $\beta = 0.5$ and $k_z = 1.0$. Thick solid lines correspond to the resolution 256^3 , while thin solid lines to that of 128^3 , both for $k_y = 0.6$. Note that on all seven panels these two curves practically overlap, which serves as a proof of convergence of our simulation results. Dashed lines represent $k_y = 0.4$, while dash-dotted lines show $k_y = 0$.

continuously distorted creating transverse gradients. Note, that the right wing of the pulse is asymmetric to the left one, this is due to the fact that its amplitude drops from 1.0 in the $x > 0$ domain to $1/\sqrt{5}$ in the $x < 0$.

- $x = 0$ cross-section: the initial Alfvénic pulse which has an asymmetric as $k_y \neq k_z$ Gaussian bell shape is split in two smaller amplitude bells traveling in two opposite directions along the magnetic field plus some elliptic-shaped wake expanding outwards in all directions. Note, that because the unperturbed density is homogeneous across the magnetic field in y -direction we do not see any distortions on the wave front with respect to the $y = 0$ line as we saw in the previous case.
- $z = 0$ cross-section: the Alfvénic pulse evolution is similar to the case of $y = 0$ cross-section. The notable difference is that through $z = 0$ cross-section pulse looks wider as $k_y = 0.6$ while $k_z = 1.0$.

Perturbation of B_y is initially absent from the system, but as it is a potential component of the kinetic counterpart, V_y , of the wave, it is soon generated and further

evolves similarly to V_y in a form of two negative and positive phase-mixed pulses traveling into two opposite directions.

At time $t = 0$ transverse and longitudinal compressive waves as well as density perturbation were absent from the system, while at time $t = 15$ as we see from Figs. 2, 3 and 4, relative density perturbation grew up to a sizeable fraction of the initial Alfvén wave amplitude. Note, that in all figures pre-factor ϵ stands to underscore the fact that the linear problem, which we study, does not depend on the initial amplitude. Thus, we use $A = 1$, while we have to bear in mind that linear approximation itself is valid for small amplitudes that is why we use small, arbitrary pre-factor ϵ in our notation. A fairly good quantity describing the generation of transverse and longitudinal compressive waves as well as density perturbations is the maximum of absolute value over the whole simulation domain. We plot this quantity for all physical variables in Fig. 5. In this figure, thick solid lines correspond to the resolution 256^3 , while thin solid lines to that of 128^3 , both for $k_y = 0.6$. It is remarkable that on all panels these two curves practically do overlap, which serves as a proof of convergence of our simulation results. The last figure in

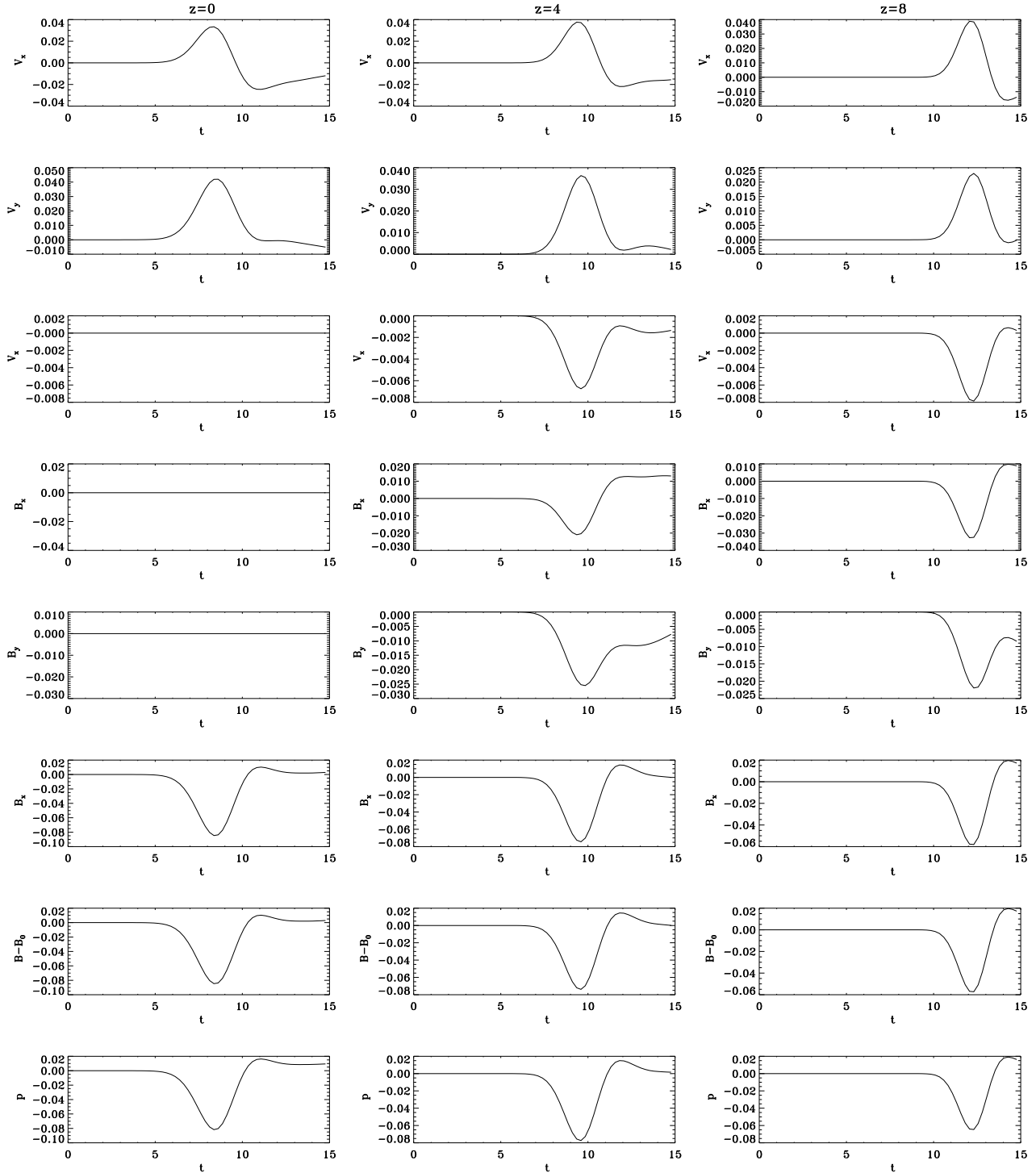


Fig. 7. All physical quantities as a function of time in a given point of space. Here, $\beta = 0.5$, $k_y = 0.6$, $k_z = 1.0$. Left column: at a point $(x=0, y=-8, z=0)$, mid column: at a point $(x=0, y=-8, z=4)$, right column at a point $(x=0, y=-8, z=8)$

the bottom row presents the maximum of absolute value over the whole simulation domain of $\text{div}\mathbf{B}$, and we indeed observe almost perfect fulfillment of the fundamental law, $\text{div}\mathbf{B} = 0$, which comes as a bonus of high-order, centered, finite difference numerical scheme. As expected, Fig. 5 shows that when $k_y = 0$ Alfvénic perturbations (V_y and B_y) are decoupled from the rest of physical quantities.

This conclusion can be deduced either from analyzing Eqs.(11)-(13) or resorting to a classic mechanical analogy of coupled pendulums. In effect, Eqs.(11)-(13) also describe three inter-coupled mathematical pendulums which are located in xOz plane. Thus, as long as we do not perturb these pendulums such that $k_y \neq 0$, they will always oscillate in the xOz plane. Thus, what we see in

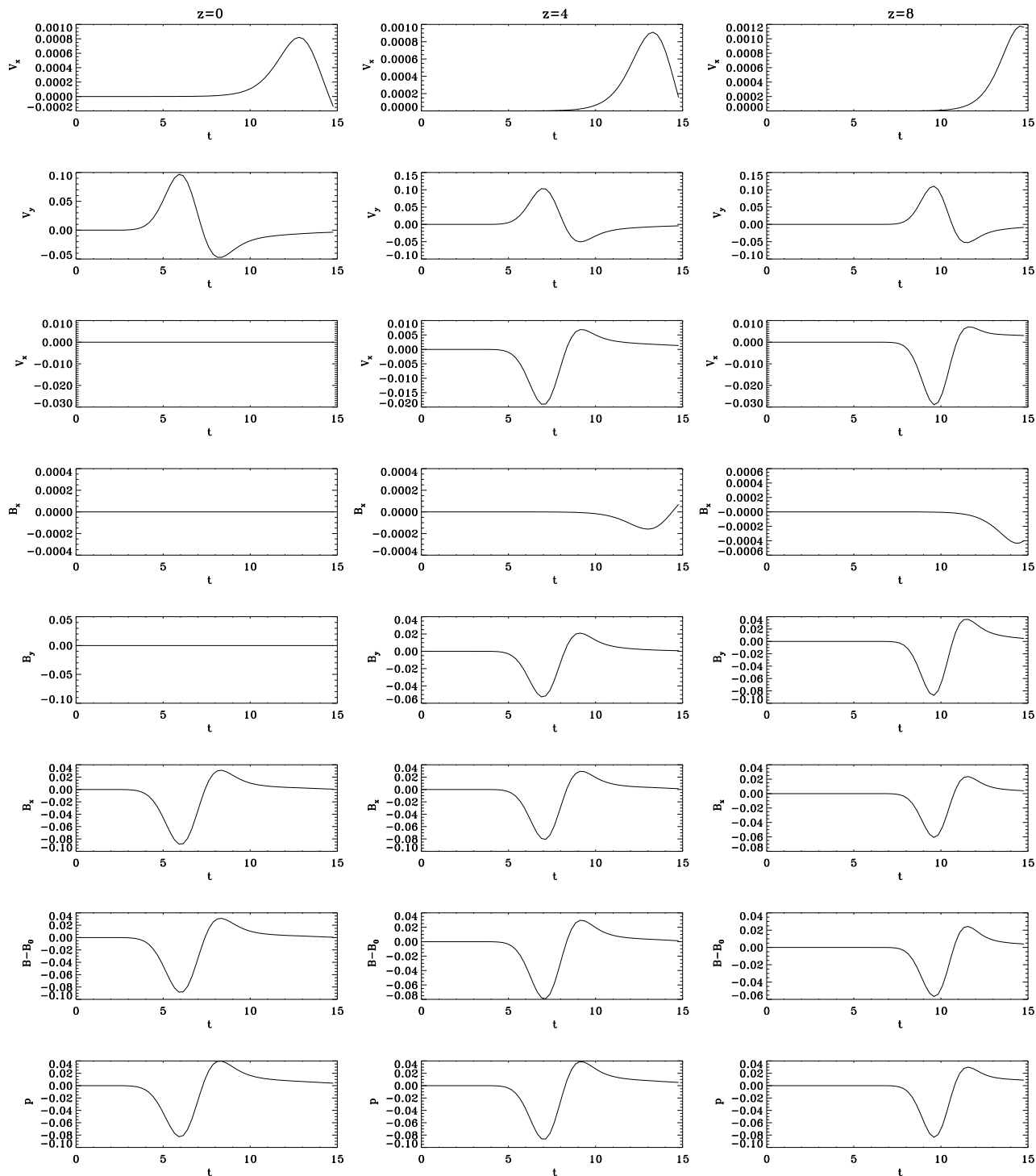


Fig. 8. All physical quantities as a function of time in a given point of space. Here, $\beta = 0.5$, $k_y = 0.6$, $k_z = 1.0$. Left column: at a point $(x=16, y=-8, z=0)$, mid column: at a point $(x=16, y=-8, z=4)$, right column at a point $(x=16, y=-8, z=8)$

Fig. 5 when $k_y = 0$ (dash-dotted lines) is that initial kinetic Alfvén perturbation (V_y) is split in half-amplitude D’Alambert’s solutions (both for V_y and B_y) and no other physical quantity is generated. However, when we switch on the coupling, $k_y \neq 0$, all transverse and longitudinal compressive physical quantities are generated. What is

noteworthy is that we observe formation of a new quasi-steady MHD state, i.e. initial Alfvénic perturbation interacts with plasma inhomogeneity, generates fast and slow magnetosonic waves (through k_y coupling) and asymptotically all three modes propagate without change in amplitude, even though phase mixing effect ($k_x \rightarrow \infty$) is in

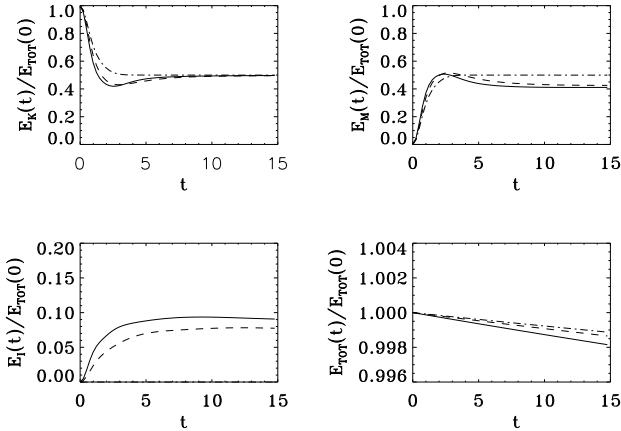


Fig. 6. Normalized kinetic, magnetic, internal and total energies as a function of time. Here, $\beta = 0.5$ and $k_z = 1.0$. Solid lines correspond to $k_y = 0.6$, while dashed and dash-dotted lines show cases of $k_y = 0.4$ and $k_y = 0$ respectively.

action all the time. Also, it can be gathered from Fig. 5 that the saturation levels of density fluctuations and incompressible fluctuations (V_y and B_y) tend to become equal as the linear coupling strength increases.

In Fig. 6 we investigate the energetics of our numerical simulation. In fact, we observe nearly perfect ($\pm 0.2\%$ error) conservation of total energy by $dt_4 dx 10$ numerical code. The major conclusion which can be drawn from this graph is that when $k_y = 0$ there is no internal (compressive) energy generation, while with the increase of k_y its saturation levels increase progressively.

In order to investigate the effect of phase mixing on the created quasi-steady MHD state, we produced time series of all physical quantities in several points of the simulation 3D box, Figs. 7 and 8. Namely, at points ($x=0, y=-8, z=0, 4, 8$), which are located in the phase mixing (spatial inhomogeneity) domain, and ($x=16, y=-8, z=0, 4, 8$), which are far away from it. The three panels (from left to the right), in effect, trace the dynamics in the z -direction (i.e. along the regular magnetic field lines). These types of data would be obtained from, for example, two satellites which are located in two different regions of solar wind. There are two noteworthy features that can be gathered from these plots: First, we see that in the phase mixing region, V_x , which is associated with the fast magnetosonic wave, attains about 40 times larger values than in the region that is far from the phase mixing region. That is a sensible result, since it is known that phase mixing efficiently generates oblique fast magnetosonic waves. Second, total magnetic field perturbation $|\mathbf{B} - \mathbf{B}_0|$ is *positively* correlated with the pressure (as well as density, which is proportional to the gas pressure) perturbation, which indeed is what was expected from the fast magnetosonic wave.

We have also performed studies of parametric space of the problem, by calculating final saturation levels of relative density perturbation as a function of linear coupling

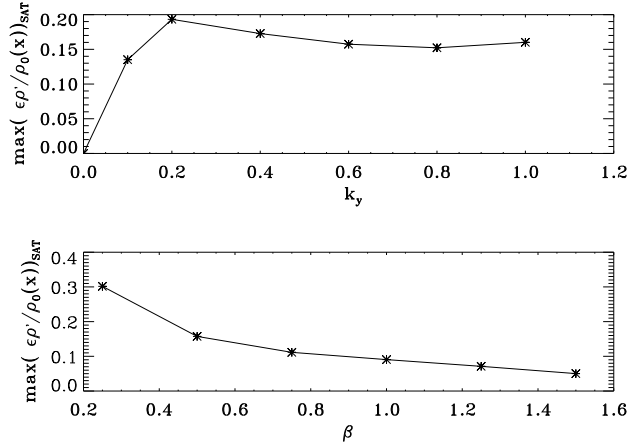


Fig. 9. Top panel: Saturation levels of maximum of the absolute values over the whole simulation box of the density perturbation as a function of k_y . Bottom panel: the same but as a function β .

strength parameter, k_y and plasma β . We gather from Fig. 9 that the final saturation levels depend weakly on k_y , while there is somewhat stronger dependence on β .

4. Conclusions

In this paper we describe in detail the effect of phase mixing on a spatially localized 3D Alfvénic perturbation.

Our numerical study of the full MHD equations established the following:

- non-zero k_y in the initial Alfvénic perturbation leads to a linear coupling to the longitudinal and transverse compressive perturbations.
- then the initial Alfvénic perturbation interacts with plasma inhomogeneity, generates fast and slow magnetosonic waves (through k_y coupling) and asymptotically all three modes propagate without change in amplitude, even though phase mixing effect ($k_x \rightarrow \infty$) is in action all the time. Thus, similarly to Roberts & Wiltberger (1995)'s results we observe a formation of a new quasi-steady MHD state. Roberts & Wiltberger (1995) performed numerical simulation of 1.5D, compressible MHD in the strongly non-linear regime. There is substantial difference, however, between our results as in their case saturation can be attributed to the action of non-linear effects, while we show that even in the linear regime, coupling between the MHD modes, which is possible only in fully 3D geometry, can result in the formation saturated quasi-steady MHD state. Roberts & Wiltberger (1995) claim that under a wide variety of conditions B and ρ become anti-correlated on average, while we show that this is not always the case (cf. Figs. 7 and 8)

- when $k_y = 0$ there is no internal (compressive) energy generation, while with the increase of k_y its saturation levels increase progressively.
- the final saturation levels of relative density perturbation depend weakly on k_y (linear coupling strength parameter), while there is somewhat stronger dependence on β .
- the saturation levels of density fluctuations and incompressible fluctuations tend to become equal as the linear coupling strength increases.

The results obtained provide a necessary basis for further studies of MHD weak turbulence in the solar wind. In the solar context, the interaction of Alfvén and magnetoacoustic modes in the three-dimensional regime of phase mixing suggests an efficient mechanism for conversion of incompressible perturbations to compressible perturbations. The latter are subject to more efficient dissipation by collisional or collisionless mechanisms. This makes the results obtained relevant to the problem of the heating of open coronal structures.

Acknowledgements. The authors are grateful to Tony Arber for valuable advice when *dt4dx10* code was written and for a number of valuable discussions. DT acknowledges financial support from PPARC. Numerical calculations of this work were performed using the PPARC funded Compaq MHD Cluster at St Andrews and Astro-Sun cluster at Warwick.

References

- Botha G.J.J., Arber T.D., Nakariakov V.M., Keenan F.P., 2000, *A&A* 363, 1186
- De Groof A., Goossens M., 2000, *A&A* 356, 724
- DeMoortel I., Hood A.W., Ireland J., Arber T.D., 1999, *A&A* 346, 641
- DeMoortel I., Hood A.W., Arber T.D., 2000, *A&A* 354, 334
- Grappin R., Léorat J., Buttighoffer A., 2000, *A&A*, 362, 342
- Hayvaerts J., Priest E.R., 1983, *A&A* 117, 220
- Hood A.W., Brooks S.J., Wright A.N., 2002, *Proc. Roy. Soc. A* (in press)
- Hood A.W., Ireland J., Priest E.R., 1997, *A&A* 318, 957
- Hood A.W., Gonzalez-Delgado D., Ireland J., 1997, *A&A* 324, 11
- Malara F., Petkaki P., Veltri P., 2000, *ApJ* 533, 523
- Malara F., Primavera L., Veltri P., 1996, *ApJ* 459, 347
- Nakariakov V.M., Roberts B., Murawski K., 1997, *Solar Phys.* 175, 93
- Nakariakov V.M., Roberts B., Murawski K., 1998, *A&A* 332, 795
- Narain U., Ulmschneider P., 1996, *Space Sci. Rev.*, 75, 453
- Petkaki P., Malara F., Veltri P., 1998, *ApJ* 500, 483
- Roberts D.A., Wiltberger M.J., 1995, *J. Geophys. Res.* 100, 3405
- Ruderman M.S., Nakariakov V.M., Roberts B., 1998, *A&A* 338, 1118
- Similon P.L., Sudan R.N., 1989, *ApJ* 336, 442
- Tsiklauri D., Arber T.D., Nakariakov V.M., 2001, *A&A* 379, 1098
- Tsiklauri D., Arber T.D., Nakariakov V.M., 2002, *A&A* submitted